Hydraulics Research
Wallingford

SPREAD OF A SURFACE THERMAL PLUME IN COASTAL WATER

Dr H O Anwar

Report No SR 140
October 1987

Registered Office: Hydraulics Research Limited, Wallingford, Oxfordshire OX10 8BA.
Telephone: 0491 35381. Telex: 848552

ACKNOWLEDGEMENTS

This report describes work funded by the Department of the Environment under Research Contract No PECD 7/6/61, for which the DoE nominated officer was Dr R P Thorogood. It is published on behalf of the Department of the Environment, but any opinions expressed in this report are not necessarily those of the funding Department. The work was carried out by Dr H O Anwar in the Tidal Engineering Department of Hydraulics Research, Wallingford under the management of Mr M F C Thorn. The author acknowledges the assistance of his colleagues Mr C B Waters, who supplied the field data, and Mr R Atkins who carried out the data analysis. Mr W Wright, Station Manager of the CEGB Fawley Power Station provided the outfall data, and Mr J F Spencer of the CERL Marine Biology Laboratory contributed helpful discussion.

ABSTRACT

This report deals with the results obtained from a field study of a thermal surface plume discharging onto a tidal current. Buoyant surface plumes in unsteady tidal current are frequently observed at many UK Power Plants, but studies of their spreads are very few. Numerical simulations require calibration using field or laboratory data. Physical simulations, on the other hand, provide simplified analysis, valuable for preliminary studies, and also give a better understanding of mixing processes. All physical simulations so far have been conducted in steady ambient currents, and of necessity, at low Reynolds numbers, their results are found to be strongly Reynolds number dependent. For this reason a re-analysis of the thermal plume data obtained in a tidal current has been found more rewarding than further laboratory experiments. From a theoretical consideration, non-dimensional parameters, describing the dilution of the plume and its spread, have been derived. Evaluations of these parameters revealed that the dilution factor along the plume axis increases with a 0.9 power of the downstream distance from the outfall. The vertical spread parameter decreases with the $-\frac{1}{2}$ power of the downstream distance, and the lateral spread remained unchanged because of plume bifurcation caused by the outfall structure.

CONTENTS

FIGURES

1 INTRODUCTION

Because of its ecological importance the mixing processes associated with the dilution and the spread of an effluent such as warm water discharging from a power plant into stagnant or steady flowing water has been studied theoretically and experimentally for many years. The object of these studies was to determine the interaction of effluent with its chemical and biological surroundings, and more immediately to insure that the affected area will meet standard regulations. Numerical simulation approaches have also been developed and refined (Refs 1 to 3), now allowing good predictions for a range of conditions (Ref 4). The difficult part of numerical modelling is the simulation of the near field flow, bearing in mind that a large mixing of an effluent with ambient water occurs in the vicinity of the outfall. The near field region has been simulated, with some success, using turbulence closure simulations, including the k-ε model (Refs 5 and 6). Numerical simulations, however, require calibration using measured data obtained from laboratory or field experiments, which also provide a better understanding of mixing processes, and simplify means of analysis useful for preliminary studies.

All physical simulations of plume spread, so far, have been carried out in laboratories with steady ambient currents at low Reynolds numbers, usually two orders of magnitude smaller than the usual field Reynolds numbers. It has been shown that plume mixing in steady ambient flows is dominated by their large-scale turbulence structures which are essentially three-dimensional and Reynolds number dependent (Ref 7). But, studies of buoyant plume mixing in an unsteady ambient current are very few, despite their frequent occurrence in nature. Hence it is felt that a field study of a thermal plume spread in an unsteady

tidal current would be more rewarding than further laboratory experiments. In the absence of adequate experimental information, a series of field measurements was undertaken when the outfall of Fawley Power Station discharged warm water onto the Solent at Southampton Water. Temperature was measured in the warm water area at various depth during a spring ebb tide.

A year later mean velocity profiles were measured within a depth of 1.50m from the bed, and also at 1m below the free surface during a spring ebb tide, in which the flow conditions must have been very close to those during the temperature measurements.

From the measured temperature data horizontal isotherms, lateral and vertical temperature profiles, position of plume axis, plume dimensions and the dilution factor along the plume axis were determined. From the velocity data the friction velocity and bed roughness were calculated.

The aim of the study presented here is to determine the terms required for the design of a surface outfall in steady and unsteady ambient currents, and also for the development of numerical simulations, in the region where buoyancy affects the mixing. It is hoped that the results will also provide a better understanding of the complex plume flow structure in the presence of buoyancy forces.

2 EXPERIMENTS

Field measurements were carried out in the Solent on 20 March 1985, when Fawley Power Station was operating at its full load, discharging cooling water onto the Solent (see Fig 1). A full description of the experimental procedure, and measurement results, are given by Waters (Ref 8).

Experimental conditions and configuration of the Power Station which are relevant to the present study will be given here.

The power station was operating at full load of 1350MW and discharging $27.3 m^3 s^{-1}$ of warm water at 12.6°C from the outfall into the Solent water at 5.8°C. The outfall headwork (see Fig 2) has its longer axis in the mean flow direction, which is generally westwards at high water and eastwards at low water, and discharges via sixteen submerged apertures each 1.7m high and 2.4m wide evenly spaced around the outfall structure. The apertures extend over 25% and 75% of the available water depth at high and low water respectively (Ref 9).

Measurements were taken during high water over a decelerating phase of the double peaks of a spring ebb tide. The plume temperatures were measured near the free surface and at 1m, 2m, 3m and 4m below, using thermistors having a time constant of $\frac{1}{2}$s and accurate to ±0.1°C from zero to 30°C (Ref 8). These sensors, together with a pressure sensing depth meter, were attached to a cable with a streamline weight at the bottom, which could hold the cable vertically at towing speeds ranging between $1 ms^{-1}$ and $1.5 ms^{-1}$. Temperatures were recorded every 10 seconds using a multi-channel print-out unit on board the tracking vessel whilst it criss-crossed the warm water area. The position of the vessel was recorded using a Motorola Minirange III microwave system (Ref 8).

The salinities and temperatures of the receiving water were measured upstream from the outfall within the 4m depth using a salinity/temperature bridge, Type MC5, which had accuracies for salinity and temperature of ±0.1 (ppt) and ±0.1°C respectively. The differences between maxima and minima of the measured scalar quantities were in the order of their sensors'

accuracies, implying that the tidal current was not stratified, neither salinity nor temperature varied during the measurements.

The outfall densimetric Froude number, $Fr=U_j/\sqrt{g'd}$, was 1.93 for Runs 1 and 2 (see also Fig 3), where U_j is the mean warm water velocity from an idealized circular outfall of diameter d=9.12m, with a discharge area equivalent to the total areas of the 16 apertures described previously. The effective acceleration due to gravity, g', will be defined later. It was not possible to determine the value of F_r for Run 3, due to not knowing the outfall temperature T_j.

3 VELOCITY MEASUREMENTS

On 21 July 1986 vertical velocity profiles were measured, within 1.50m of the bed, upstream from the outfall using Braystoke current meters set at six elevations of 0.2m vertical intervals starting at 0.2m from a base-plate resting on the bed. Velocity, averaged over five minutes period, was measured at these six elevations simultaneously during the decelerating phase of a spring ebb tide. The results indicate that the measured profiles were logarithmic of the following form:

$$\frac{U}{U_*} = \frac{1}{k} \ln \left(\frac{z-d}{z_o}\right) \qquad (1)$$

in which the mean velocity U was measured at elevation z, and the friction velocity $U_* = (\tau_o/\rho)^{\frac{1}{2}}$, τ_o being the bed shear and ρ the mass density of water. The roughness length z_o characterizes the effect of the bed roughness and k is the Karman constant of 0.4; in agreement with the experimental results obtained in a simulated tidal flow (Ref 10). In Eq (1) d is the height of a zero-plane measured from the base-plate, indicating the depth of a virtually stationary water layer trapped between the roughness elements (Ref 11).

Equation (1) was fitted to the measured profiles by a least squares regression within 95% confidence limits (Ref 11), from which U_* and z_o were evaluated by choosing a value of d to obtain a correlation coefficient R≈0.996 (Ref 11). The calculated values of U_* and z_o, together with variations of the water depth, and of the mean velocity at 1m below the free surface are shown in Figure 3. As may be seen the friction velocity U_* is time-dependent, and the drag coefficient $C_D = (\frac{U_*}{\bar{U}})^2$ also varied with time, where $\bar{U}$ is the mean velocity at z=1.50m. Figure 3 further shows that the roughness length z_o is variable, with a trend similar to that of the friction velocity U_*. The bed material was fine sand with d_{50} = 0.25mm, covered with gravel having the average size d_g = 30mm. It was found that the ratio $\frac{d}{d_g} \approx 1.3$ (for d see Eq 1) much higher than 0.7 found by Jackson (Ref 1) for steady flows over laboratory and field roughness.

4 TEMPERATURE DISTRIBUTIONS

From the measured temperature data horizontal isotherms were determined for experimental Runs 1 to 3 (see also Fig 3). The results near the free surface and 1m below are shown in Figures 4 to 6, in which $\Delta T=T-T_a$ is the excess temperature, where T and T_a are the plume temperature and the ambient current temperature respectively. Figures 4 to 6 show that the plume is divided in two parts almost near the outfall, due to a division of the ambient current by the outfall headwork, which can also be detected from Figure 2. The branched plume merged again later, producing a single plume when the outfall effect had diminished which will be discussed later. In Figures 4 to 6 are also shown the right-hand (R.H) and the left hand side (L.H) plume axes, which are the loci of

the maximum temperatures in the divided plume. The variation of the distance between these axis in the mean flow direction will be given later. Figures 4 to 6, together with the isotherm patterns at other depths disclose that the excess temperature ΔT decreases with increasing depths below the free surface which will be shown later. In Figures 4 to 6 are also shown the tracking courses, starting at a distance of about 180m downstream from the outfall.

5 LATERAL TEMPERATURE PROFILES

From the measured data lateral temperature profiles along each tracking course were determined, and the results in their normalized forms at two depths are shown in Figures 7 and 8 for Runs 1 and 2 respectively. In Figures 7 and 8, y, denotes the lateral distance measured from the relevant plume axis, and δ_1 is a lateral length scale, so that when $y=\delta_1$ the normalized excess temperature $\frac{T-T_a}{T_m-T_a} = \frac{1}{2}$, where T_m occurs at the plume axis. The solid line in Figures 7 and 8 is the Gaussian profile expressed by:

$$\frac{T-T_a}{T_m-T_a} = \exp\left[-0.693\left(\frac{y}{\delta_1}\right)^2\right] \qquad (2)$$

Although there is some scatter, it is reasonable to assume that the normalized profiles follow Equation (2), except in the warm water region (dashed line) occurring between the R.H and L.H side plumes. The occurrence of a warm water region, which will be discussed later, indicates that the behaviour of the branching and merging plume of the present study differs from those of strong buoyant bifurcated plumes in steady ambient currents studied by others (Refs 13 and 14), which showed that the separation, starting at some distance from the outfall, increased with

increasing downstream distance from the outfall, and each branch behaved much like a single plume. Figures 4 to 6 show that the plume branched almost at the outfall headwork.

6 VERTICAL TEMPERATURE PROFILES

Vertical temperature profiles were determined along the R.H and L.H side plume axes (see also Figs 4 to 6), and the results in their normalized forms are shown in Figures 9 and 10 for Runs 1 to 3; the downstreams distance x was measured along the relevant plume axis. In Figures 9 and 10, $T_{max}-T_a$ is the maximum excess temperature, occurring near the free surface, and δ_z is a depth scale at which $\frac{Tm-Ta}{T_{max}-Ta} = \frac{1}{2}$. The solid lines are the Gaussian profile of the following form:

$$\frac{T_m-T_a}{T_{max}-T_a} = \exp\left[-0.693\left(\frac{z}{\delta_z}\right)^2\right] \qquad (3)$$

in which z is measured from the free surface vertically downwards. As may be seen the normalized profiles agree reasonably well with Eq (3).

7 ANALYSIS

The results shown in Figures 7 to 10 indicate that the temperature profiles in the lateral and vertical directions are geometrically similar at various downstream distances, x, with δ_l, δ_z, (T_m-T_a) and $(T_{max}-T_a)$ as scale quantities (see also Eqs 2 and 3). Furthermore it has been shown by Eq (1) that the friction velocity U_* and the roughness length z_o can be used as scale quantities to specify the near-bed flow; with the conclusion that the flow within the tracking area is similar to that of a turbulent

boundary layer type flow and thus is self-similar because it depends solely on the instantaneous parameters and not on the flow history. Hence it is legitimate to use dimensional analysis to derive a set of non-dimensional parameters from an appropriate set of independent variables to describe the spread of a buoyant surface plume in an unsteady ambient current. These independent variables are: the outfall densimetric Froude number F_r defined previously, the unsteady ambient velocity U_a, (see Fig 3) with temperature T_a, the warm water velocity U_j with temperature T_j and finally the acceleration due to gravity, g. When the density difference, arising from buoyancy produced by the temperature excess $T_j - T_a$, is small, it is customary to replace g by the effective gravitational acceleration $g' = g\frac{\rho_a - \rho_j}{\rho_a}$, where ρ_a and ρ_j are the mass densities of the ambient current and the warm water at the outfall respectively. The dependent variables are: the dilution factor S (defined later) along the plume axis, and the plume dimensions δ_z and δ_l. Dimensional analysis then leads to the following expressions:

$$S = \frac{T_j - T_a}{T_m - T_a} = f_1 \left(\frac{U_j}{U_a} \frac{g'x}{U_a^2}, F_r \right) \tag{4}$$

$$\frac{g'\delta_z}{U_a^2} = f_2 \left(\frac{U_j}{U_a} \frac{g'x}{U_a^2}, F_r \right) \tag{5}$$

$$\frac{g'\delta_l}{U_a^2} = f_3 \left(\frac{U_j}{U_a} \frac{g'x}{U_a^2}, F_r \right) \tag{6}$$

in which f_1 to f_3 denote universal functions of the arguments in parenthesis. It is worth mentioning that the first term on the right-hand side of Eqs (4 to 6) can be written in terms of travelling time $T = x/U$, and thus becomes

$\frac{U_j g' T}{U_a U_a}$, where U_a is time-dependent. Further more it should be pointed that U_a in Eqs (4 to 6) can be replaced by the friction velocity U_* (see Fig 2), but in practice U_a, at a depth 1m or 2m, is usually measured.

8 PLUME DILUTION

The dilution factor S defined by Eq (4) was evaluated from the data obtained for the R.H and L.H plume axes at three depths of Runs 1 and 2 (see also Figs 4 and 5), and the results are shown in Figure 11 in which $R = U_j/U_a$ is the velocity ratio. Figure 11 shows that the evaluated data fall within a narrow band regardless of the unsteadiness of the ambient current. The solid line in Figure 11 indicates an empirically fitted curve expressed by:

$$S = 0.7 \left(R \frac{g'x}{U_a^2}\right)^{0.9} \qquad (7)$$

which indicates that the dilution factor S increases with a 0.9 power of the normalized downstream distance from the outfall. It is to be noted that the densimetric Froude number F_r (see Eq 4) has not occurred in Fig 11 and in Eq (11), because $F_r = 1.93$ remained unchanged during Runs 1 and 2. There are very few studies of surface plumes in unsteady ambient current; more measurements are desirable for comparison, and also to determine the F_r - effect.

The dilution factor S has been evaluated for the steady ambient current of the Great Lakes at the Point Beach Power Plant with $F_r = 1.50$ (Ref 15) and the Lake View Generating Station, $F_r = 3$, (Refs 1 and 16) were discharging warm water onto Lake Michigan and Lake Ontario respectively. The results are shown in Figure 12 with an empirically fitted curve (solid line) of the following form:

$$S = 0.088 \left(R \frac{g'x}{U_a^2}\right)^{\frac{1}{2}} \qquad (8)$$

It is interesting to note that although the value of F_r for each power plant remained practically constant its variation did not affect the results shown in Fig 12 and Eq (8). By comparing Eq (7) with Eq (8) (see also Figs 11 and 12) it can be concluded that both the plume bifurcation and the flow unsteadiness caused a large increase in plume dilution. On the other hand it was shown (Refs 7 and 10) that the unsteadiness of flow, affecting the mechanism of turbulence, increased the plume dilution, but not to the extent given in Figure 11. This leads to the conclusion that the plume bifurcation of the present study created a substantial increase in plume dilution.

9 PLUME SPREADS

Non-dimensional parameters describing the vertical plume spread given in Eq (5) were evaluated from the measured data and the results, together with an empirically fitted curve (solid line) of the following form, are shown in Figure 13:

$$\frac{g'\delta_z}{U_a^2} = 0.035 \left(R \frac{g'x}{U_a^2}\right)^{-\frac{1}{2}} \qquad (9)$$

Figure 13 and Eq (9) disclose that the plume became thinner with increasing downstream distance parameter, $R \frac{g'x}{U_a^2}$, implying that buoyancy and the occurance of a warm water region (see Figs 7 and 8) inhibit the vertical growth. Our knowledge about the effect of buoyancy on turbulent mixing is severely limited; further work in this area is required.

Non-dimensional parameters for the lateral plume spread given in Eq (6), were evaluated from the measured data taken in the outer regions of the plume. It was found that the lateral spread parameter, $\frac{g'\delta_l}{U_a^2}$

remained unchanged as the distance parameter, $R \frac{g'x}{U_a^2}$, increased.

This is due to the occurrence of a warm water region between the R.H and L.H side plumes, described previously (see also Figs 7 and 8). The width of the warm water region, defined by the distance, D, between the R.H and L.H side plume axes (see also Figs 4 to 6), increased with increasing downstream distance x and then decreased when the outfall effect diminished as may be seen in Fig 14, in which $\frac{g'D}{U_a^2}$ and $R \frac{g'x}{U_a^2}$ denote normalized parameters for D and x respectively (see also Eqs 4 to 6). Fig 14 shows that when $R \frac{g'x}{U_a^2} < 10$ the distance parameter, $\frac{g'D}{U_a^2}$ increased with increasing downstream distance parameter $R\, g'x/U_a^2$, expressible by the following empirical relationship (solid line):

$$\frac{g'D}{U_a^2} = \ln \left(0.77\ R \frac{g'x}{U_a^2}\right)^{1.45} \qquad (10)$$

The left-hand side parameter of Eq (10) then decreased slowly with further increase of downstream distance parameter, implying the diminishing effect of the outfall structure, the dashed line in Fig 14 is drawn to guide the eye.

10 CONCLUSIONS

The spread of a warm water plume discharging from a power plant onto coastal water during a spring ebb tide was measured with the following results:

1. The warm water plume was divided into two parts due to a division of the ambient current by the outfall headwork.

2. The two parts of the plume merged again, when the outfall effect had diminished.

3. Between the divided plume there occurred an inner warm water region in which the longitudinal variation of temperature was less than that occurring along the R.H and L.H plume axes.

4. The width of the warm water region increased with increasing distance downstream from the outfall, it then decreased as the outfall effect diminished.

5. The lateral and the vertical temperature profiles were of the Gaussian form.

6. The dilution factor increased with a 0.9 power of the downstream distance parameter, disclosing a large increase in plume dilution in comparison with non-bifurcated plumes in steady currents.

7. The vertical spread parameter decreased with the $-\frac{1}{2}$ power of the downstream distance parameter.

8. The lateral spread parameter of the outer region of the plume remained unchanged due to the occurrence of an inner warm water region.

11 REFERENCES

1. Evans-Roberts, D J. Integral plume model for surface discharge, Hydraulics Research Station, Wallingford, Report No IT 186, November 1978.

2. Miles, G V. Formulation and development of a multi-layer model of estuarine flow, Hydraulics Research Station, Wallingford, Report No IT 155, May 1977.

3. Cooper, A J. Development and application of 3-D DAP numerical model of estuarines. Hydraulics Research Ltd, Report No SR 38, March 1985.

4. Odd, N V M. Modelling the dispersal of effluent in tidal waters, Hydraulics Research Ltd, Report No SR 47, April 1985.

5. McGuirk, J J and Rodi, W. Mathematical modelling of three-dimensional heated surface jets. Journal of Fluid Mechanics, Vol 95, 1979, pp 609-633.

6. Launder, B E, Reece, G J and Rodi W. Progress in the development of a Reynolds stress turbulence closure model. Journal of Fluid Mechanics, Vol 68, 1975, pp 537-567.

7. Anwar, H O. The flow of a surface jet in a cross-flow. Journal of Hydraulic Engineering. Vol 113, No 7, July 1987, pp 892-904.

8. Waters, C B. Field measurement of thermal plumes, Hydraulics Research Ltd, Report No SR 20, March 1985.

9. Spencer, J F. Temperature studies related to the dispersal the cooling water discharge from Fawley

Power Station, Memorandum, Symposium on Marine Science and Electricity Generation in Southampton Water, Central Electricity Research Laboratories, LM/BIOL/001, August 1975, pp 17-32.

10. Anwar, H O and Atkins, R. Turbulence measurements in simulated tidal flow. Proc American Society of Civil Eng. Hydraulics Division, Vol 106, No HY8, August 1980, pp 1273-1289.

11. Anwar, H O. Low Reynolds number turbulent flow in laboratory flume. Journal of Engineering Mechanics, Proc. American Society of Civil Eng. Vol 112, No 1, January 1986, pp 55-69.

12. Jackson, P S. On the displacement height in the logarithmic velocity profile. Journal of Fluid Mechanics, Vol III, 1981, pp 15-25.

13. Abdelwahed, M S and Chu, V H. Bifurcation of buoyant jets in cross-flow. Dept of Civil Engineering, McGill University, Tech Report 78-1, 1978.

14. Turner, J S. A comparison between buoyant vortex rings and vortex pairs, Journal of Fluid Mechanics, Vol 7, 1960, pp 419-432.

15. Kuhlman, J M and Prahl, J M. Buoyant rectangular surface thermal plumes, Journal Great Lakes Research, December 1976, pp 340-356.

16. Elliot, R V and Harkness, D G. A phenomenological model for the prediction of thermal plumes in large lakes, the 15th Conference on Great Lakes Research, April 5-7, 1972.

FIGURES.

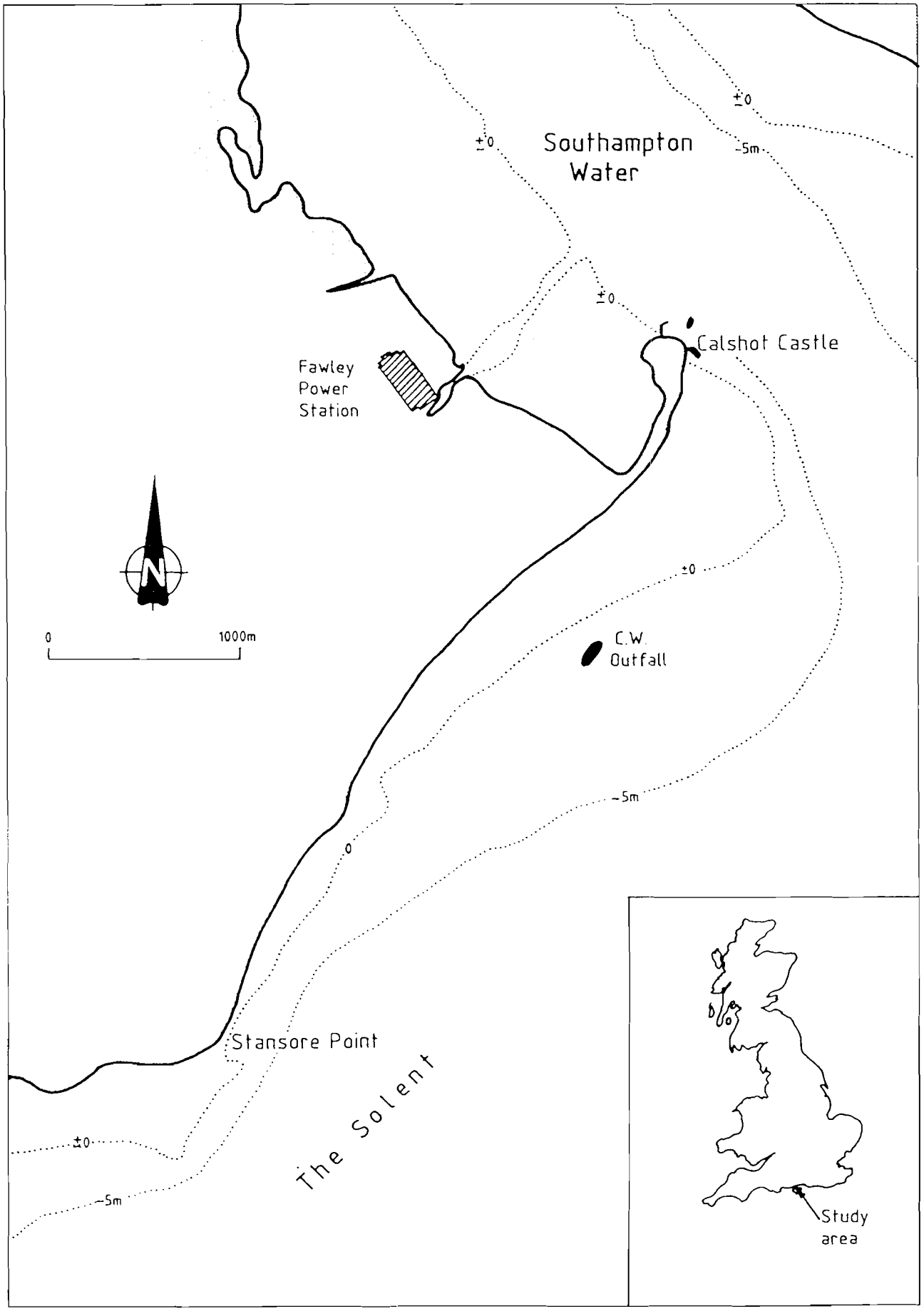

Fig 1 Experimental site and outfall location

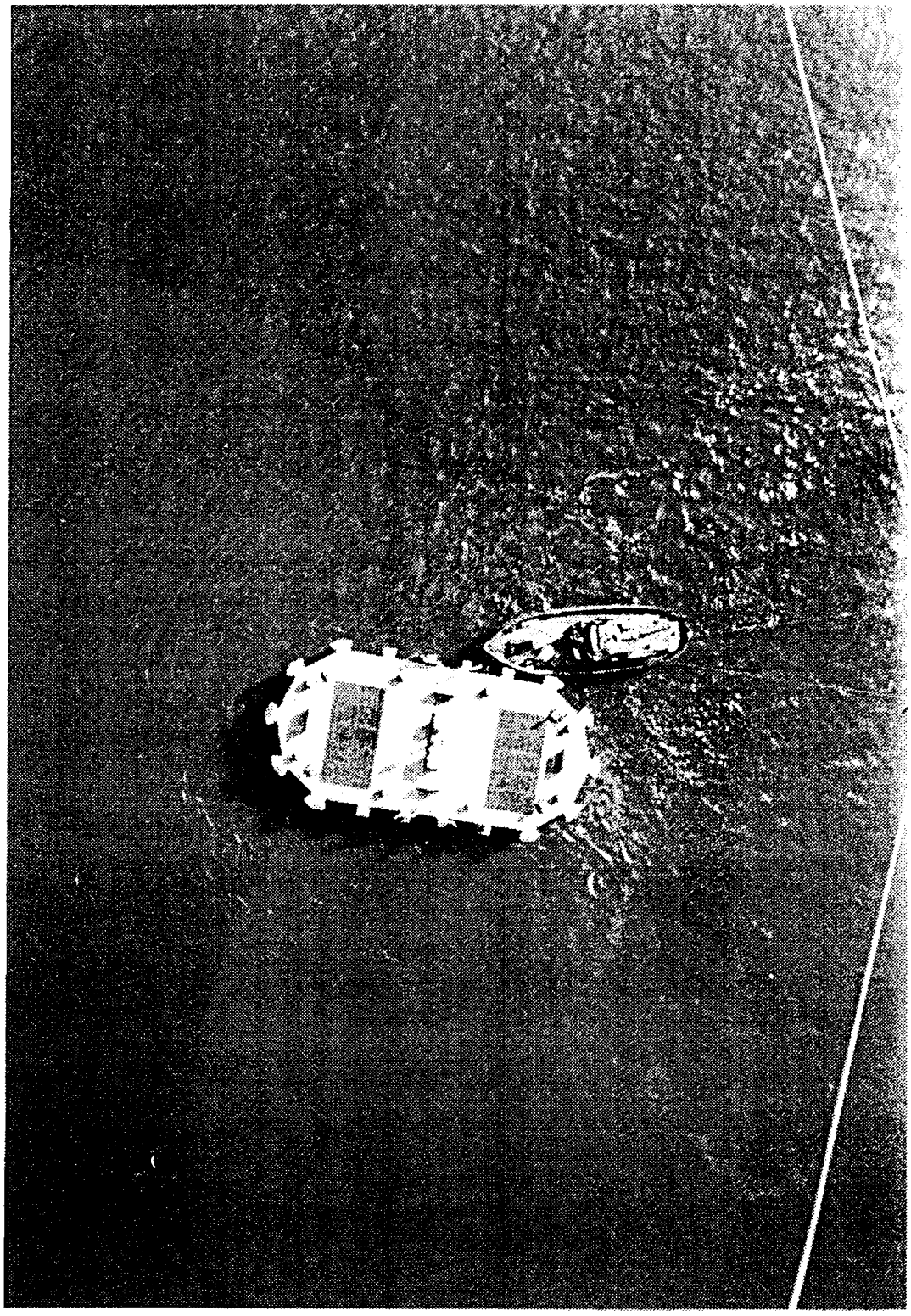

Fig 2 Aerial photograph of the outfall headwork and the ambient current

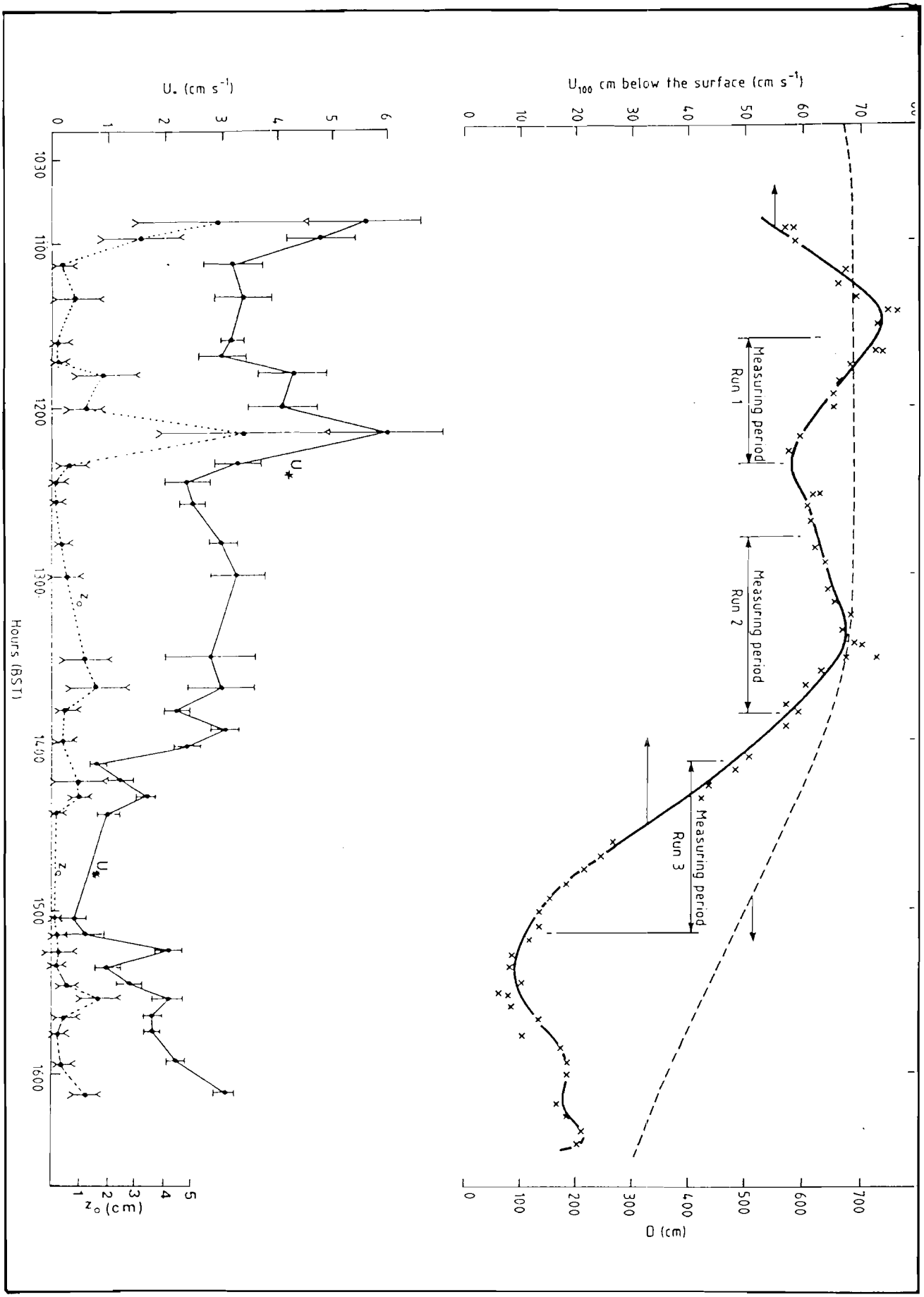

Fig 3 Variation of the mean velocity U at 1m below the free surface, water depth D, the friction velocity U* and the roughness length z_0

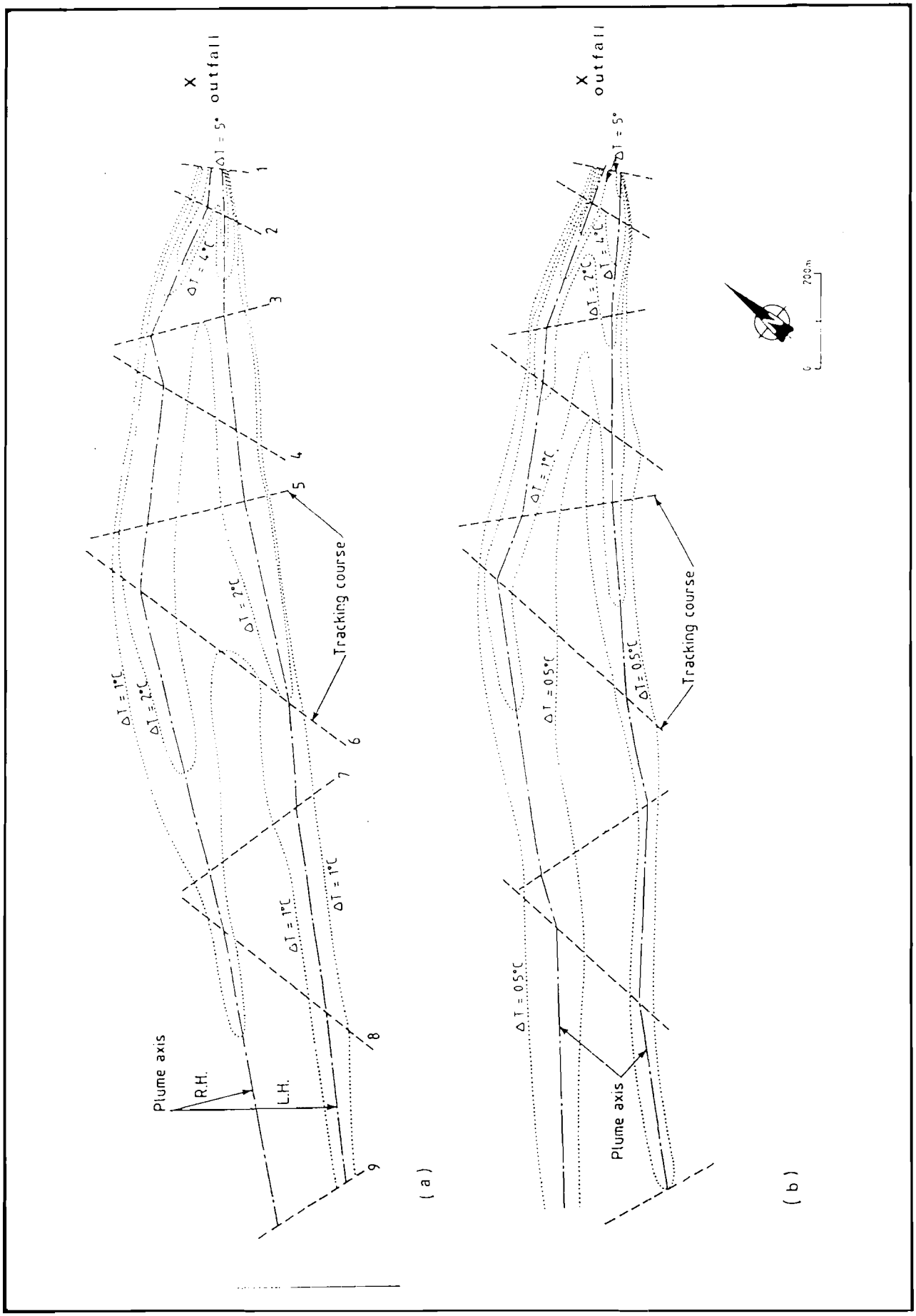

Fig 4 Horizontal isotherms (a) near the free surface (b) 1m below, for Run 1 (see also Fig 3)

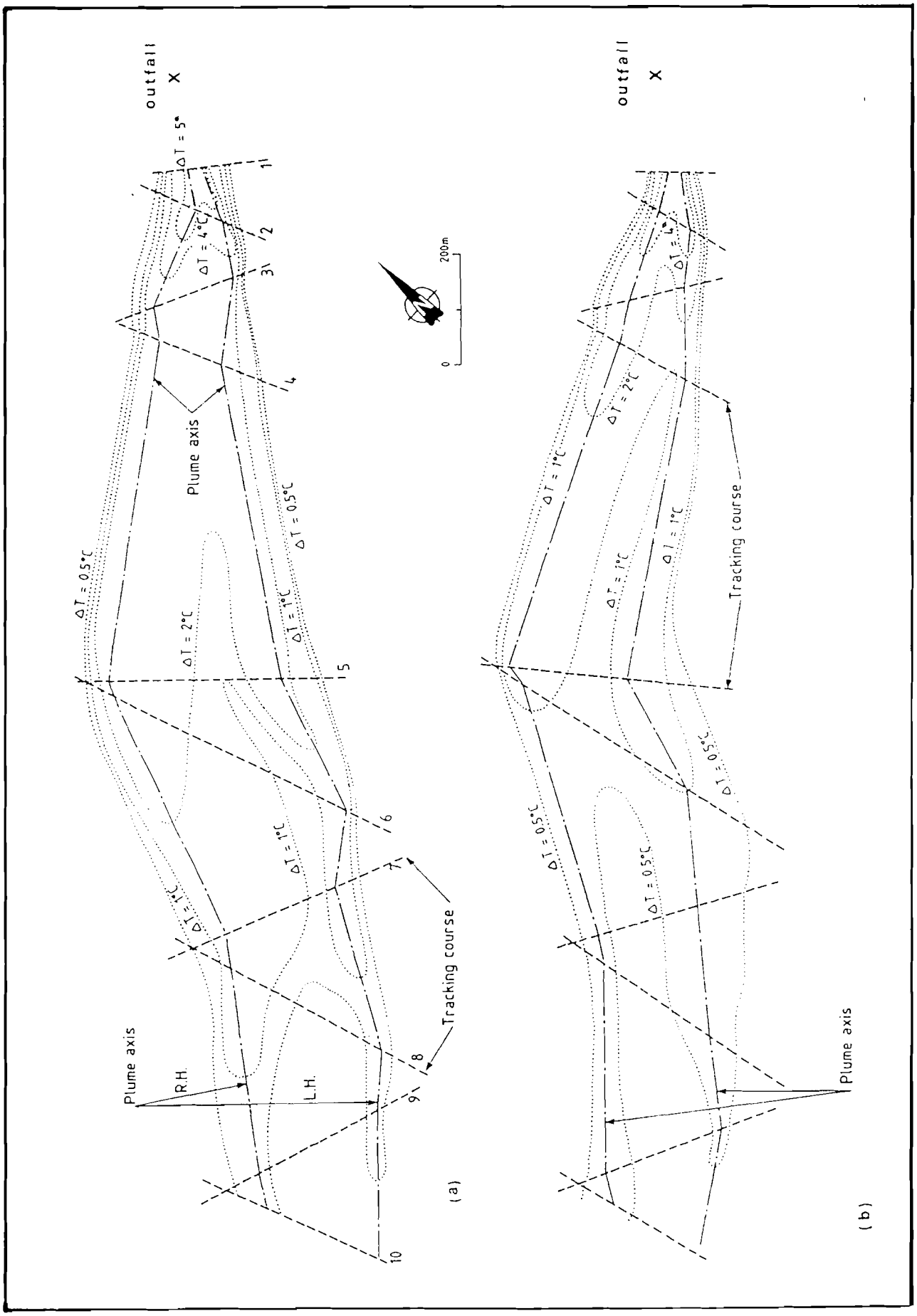

Fig 5 Horizontal isotherms (a) near the free surface (b) 1m below, for Run 2 (see also Fig 3)

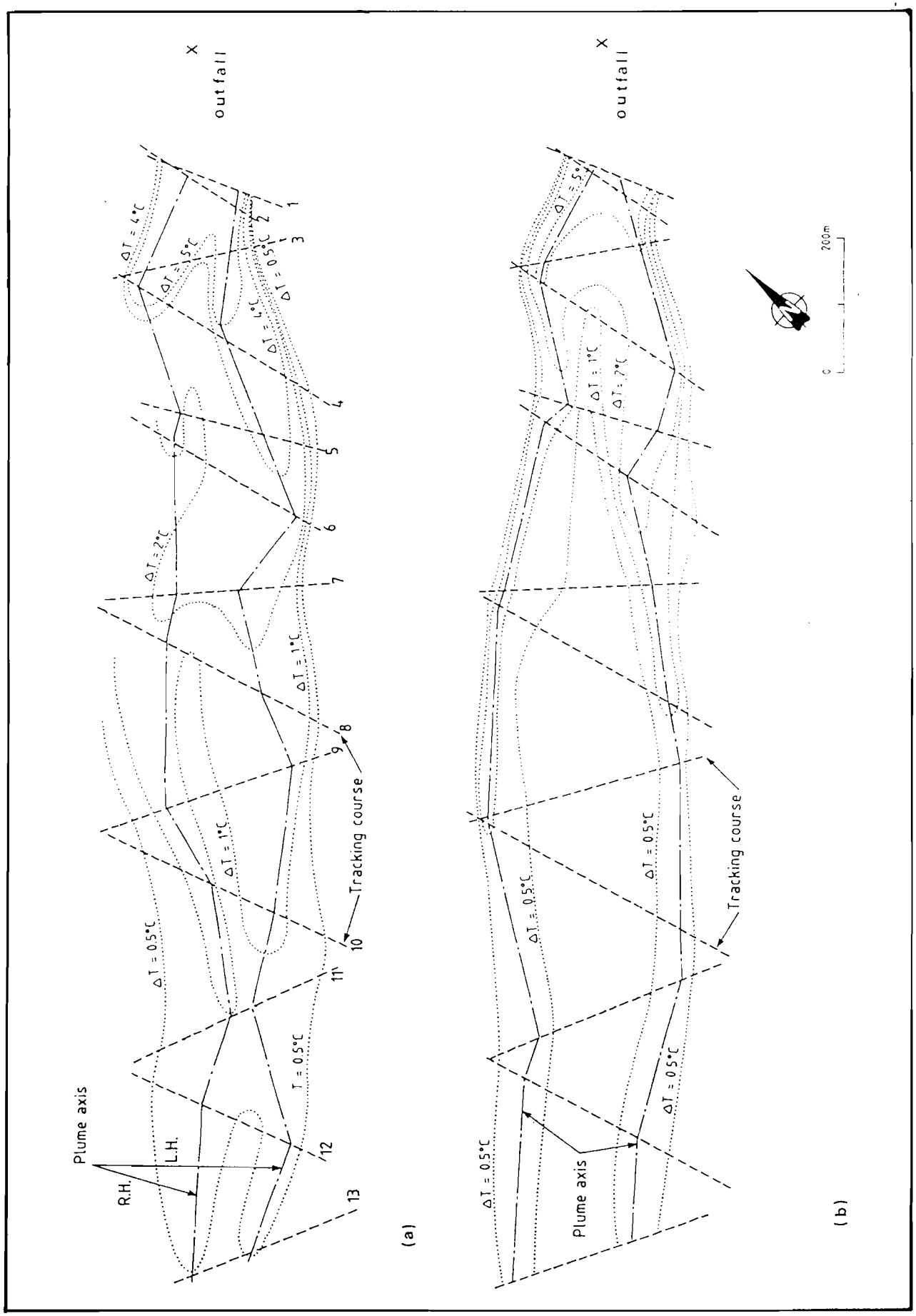

Fig 6 Horizontal isotherms (a) near the free surface (b) 1m below, for Run 3 (see also Fig 3)

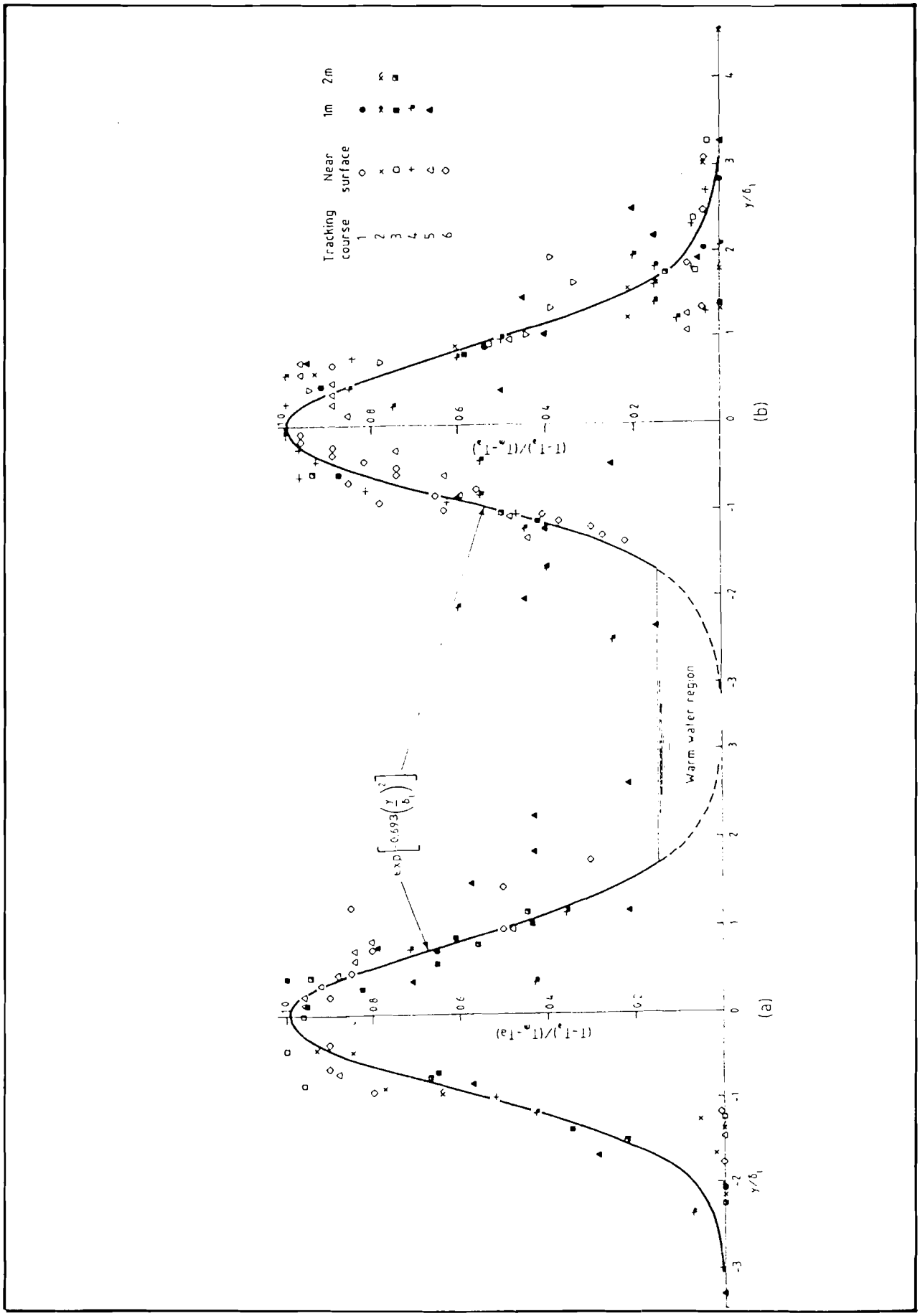

Fig 7 Normalized lateral temperature profiles for Run 1 (see also Fig 4)

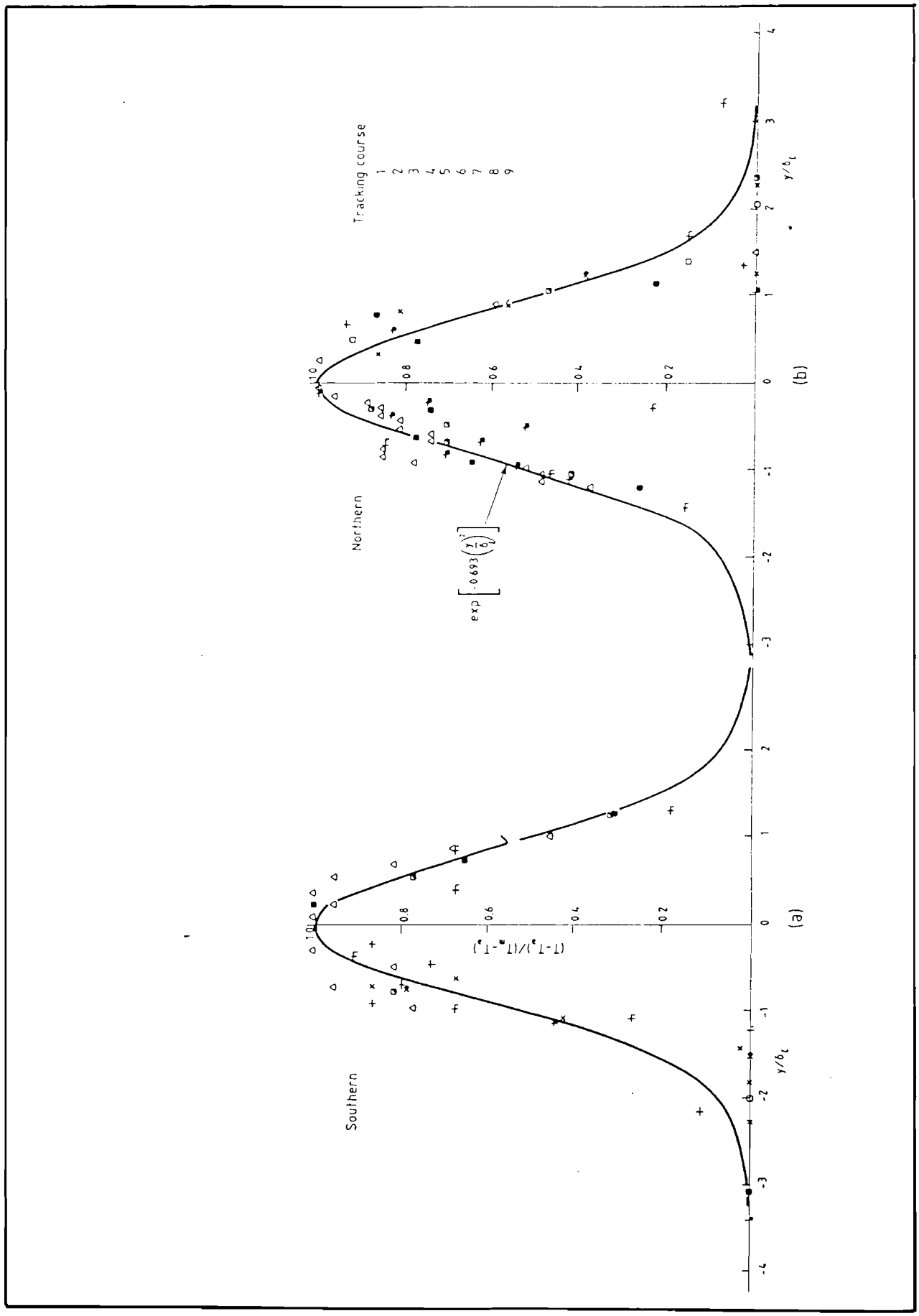

Fig 8 Normalized lateral temperature profiles for Run 2 (see also Fig 4)

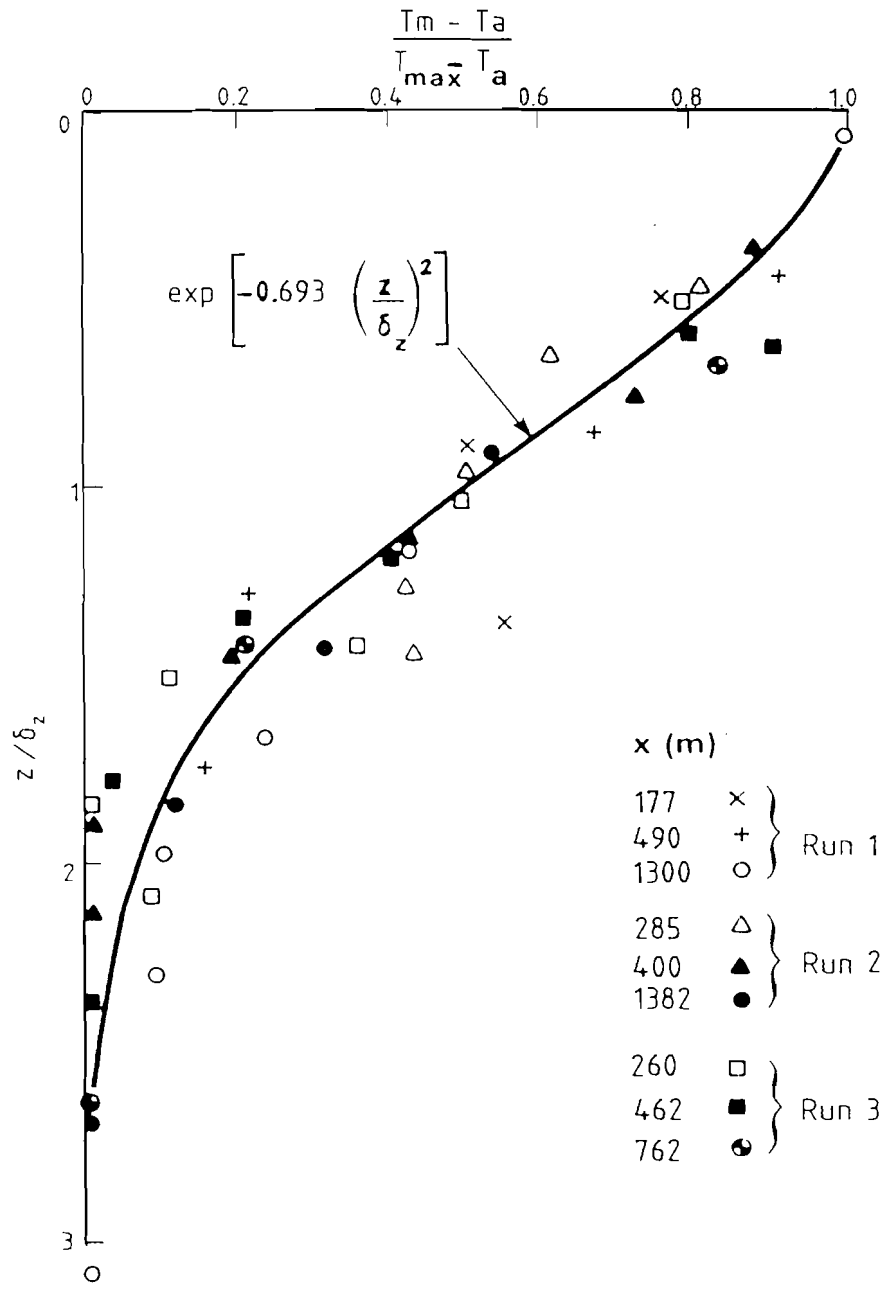

Fig 9 Normalized vertical temperature profiles along the right-hand side plume axis (see also Fig 4)

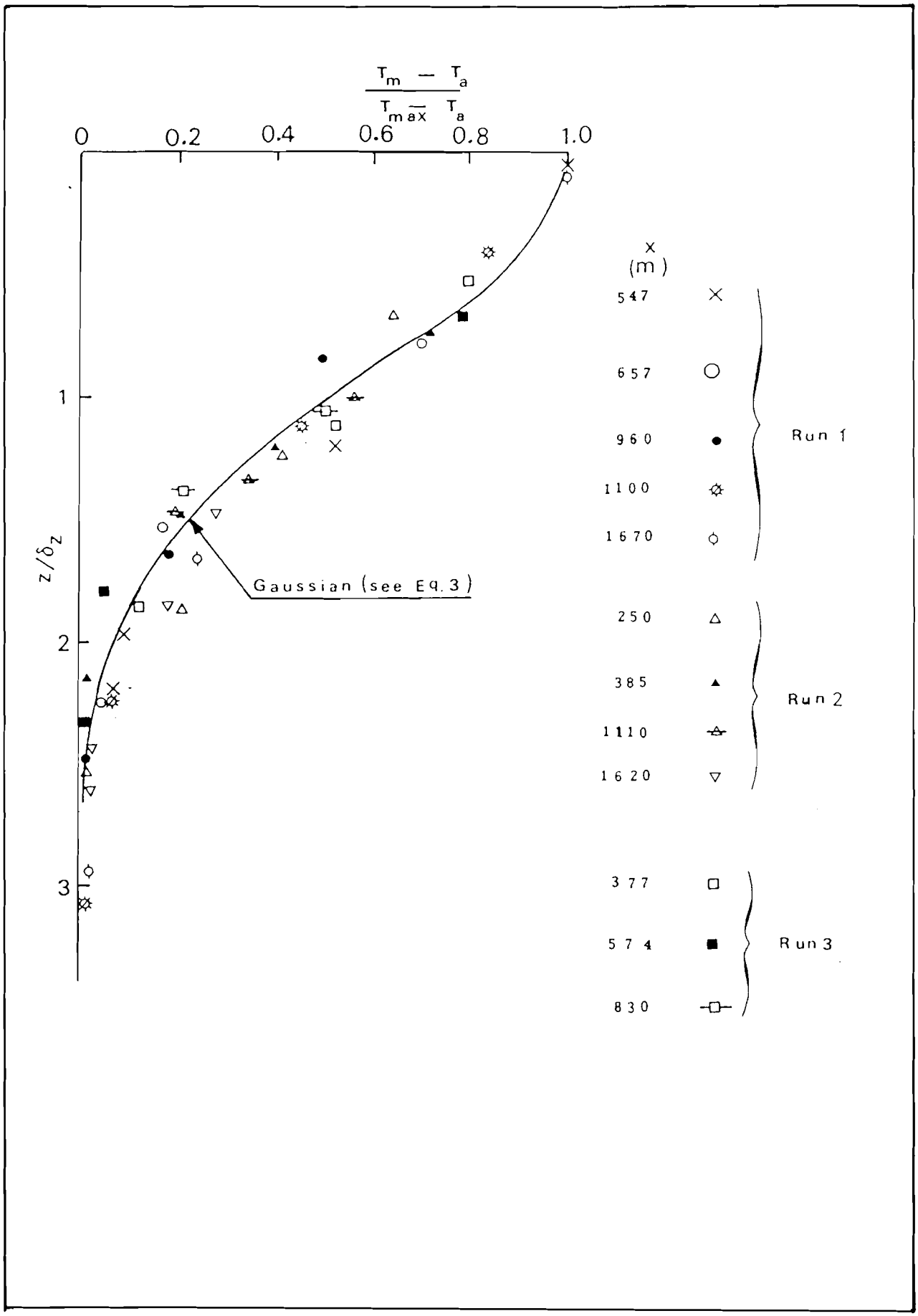

Fig 10 Normalized vertical temperature profiles along the left-hand side plume axis (see also Fig 4)

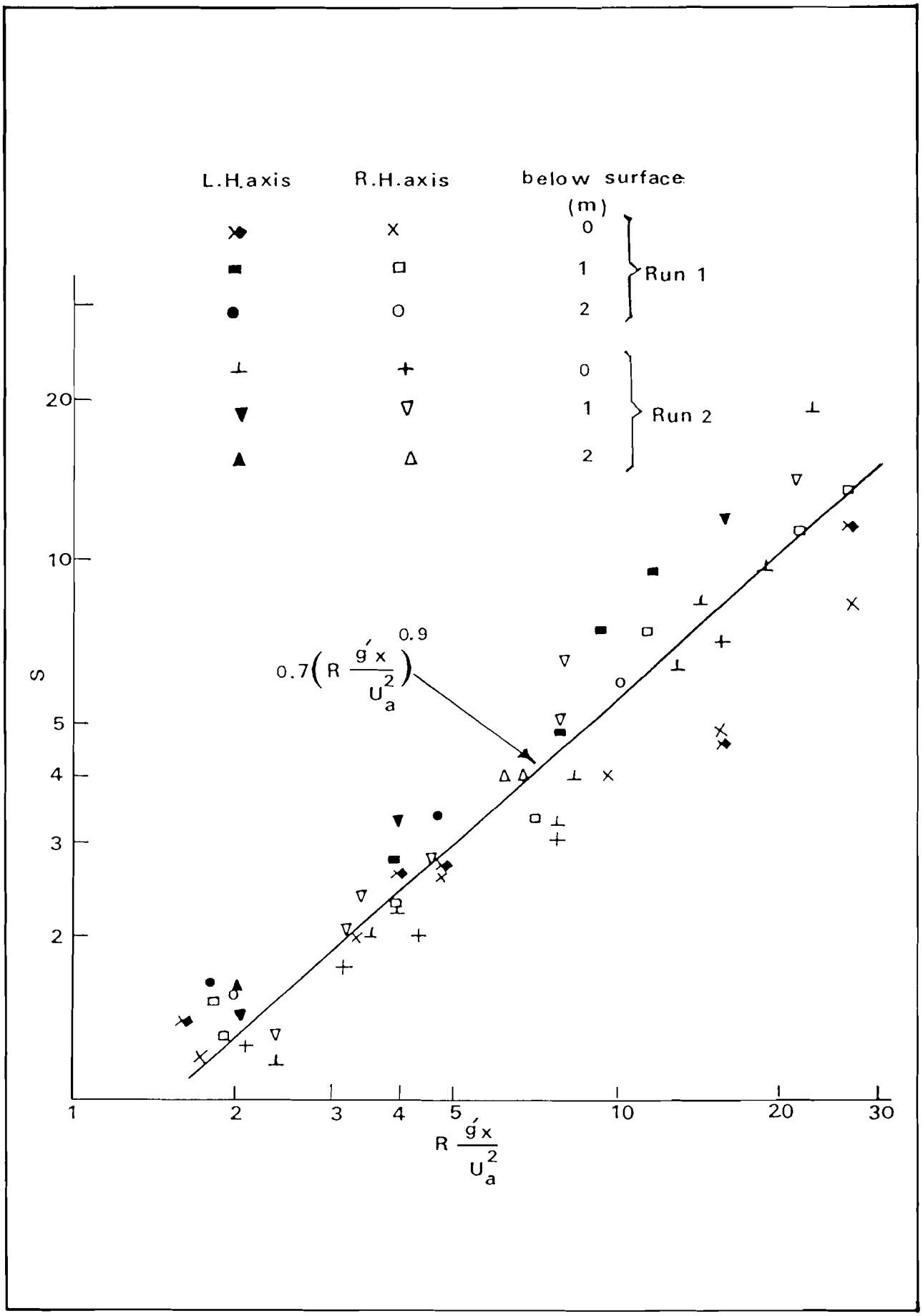

Fig 11 Plume dilution at the right-hand and left-hand side plume axes

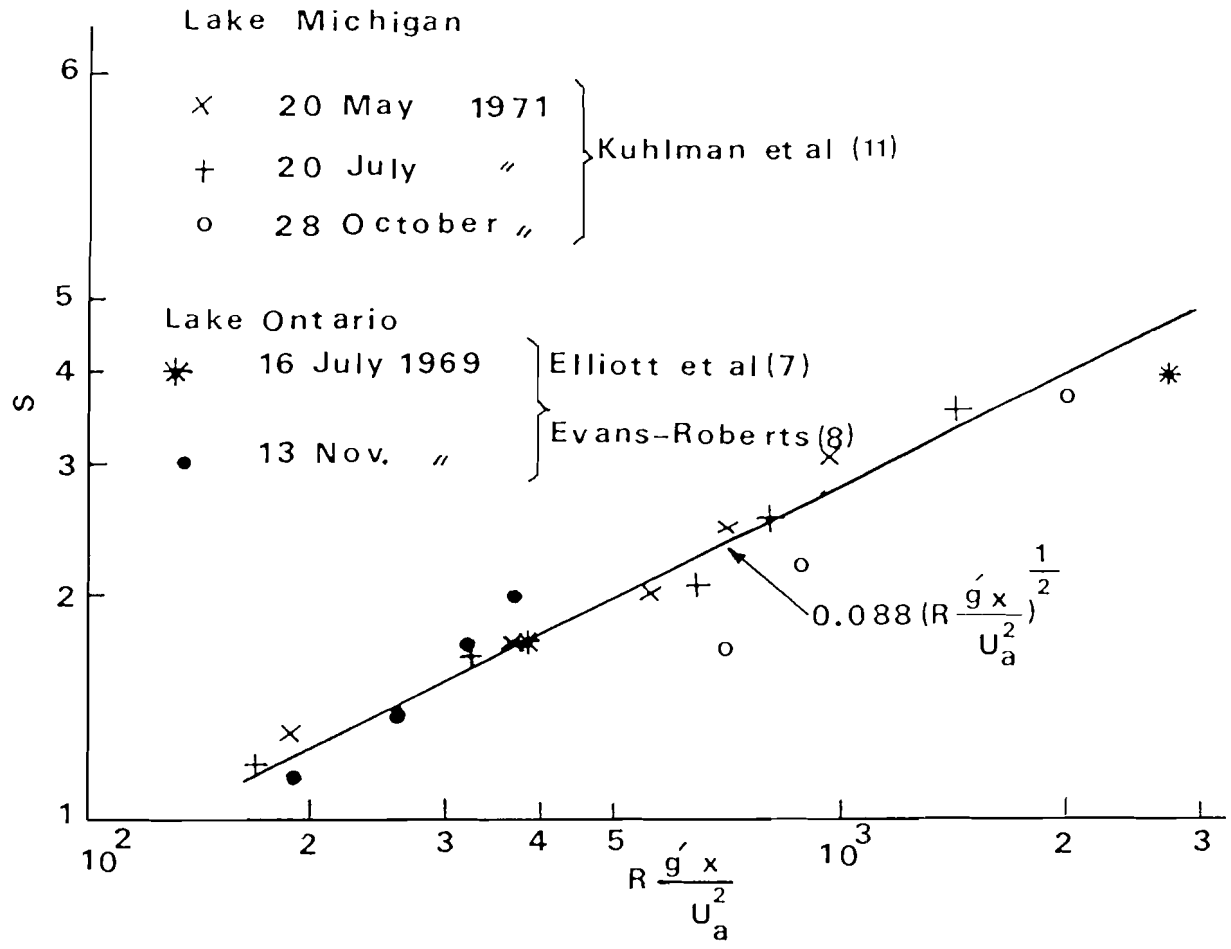

Fig 12 Plume dilution of non-bifurcated plumes in steady ambient currents

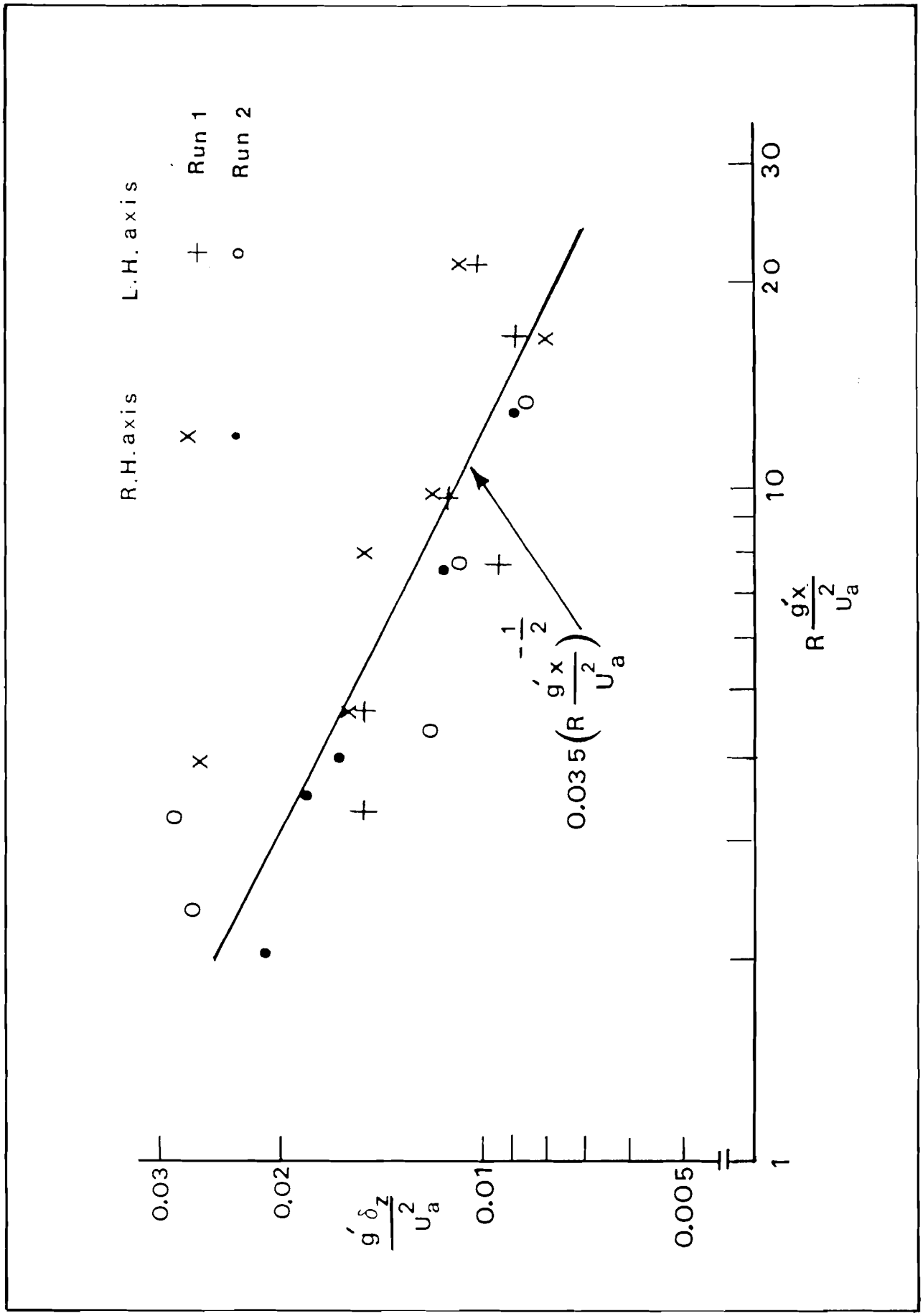

Fig 13 Vertical plume spreads

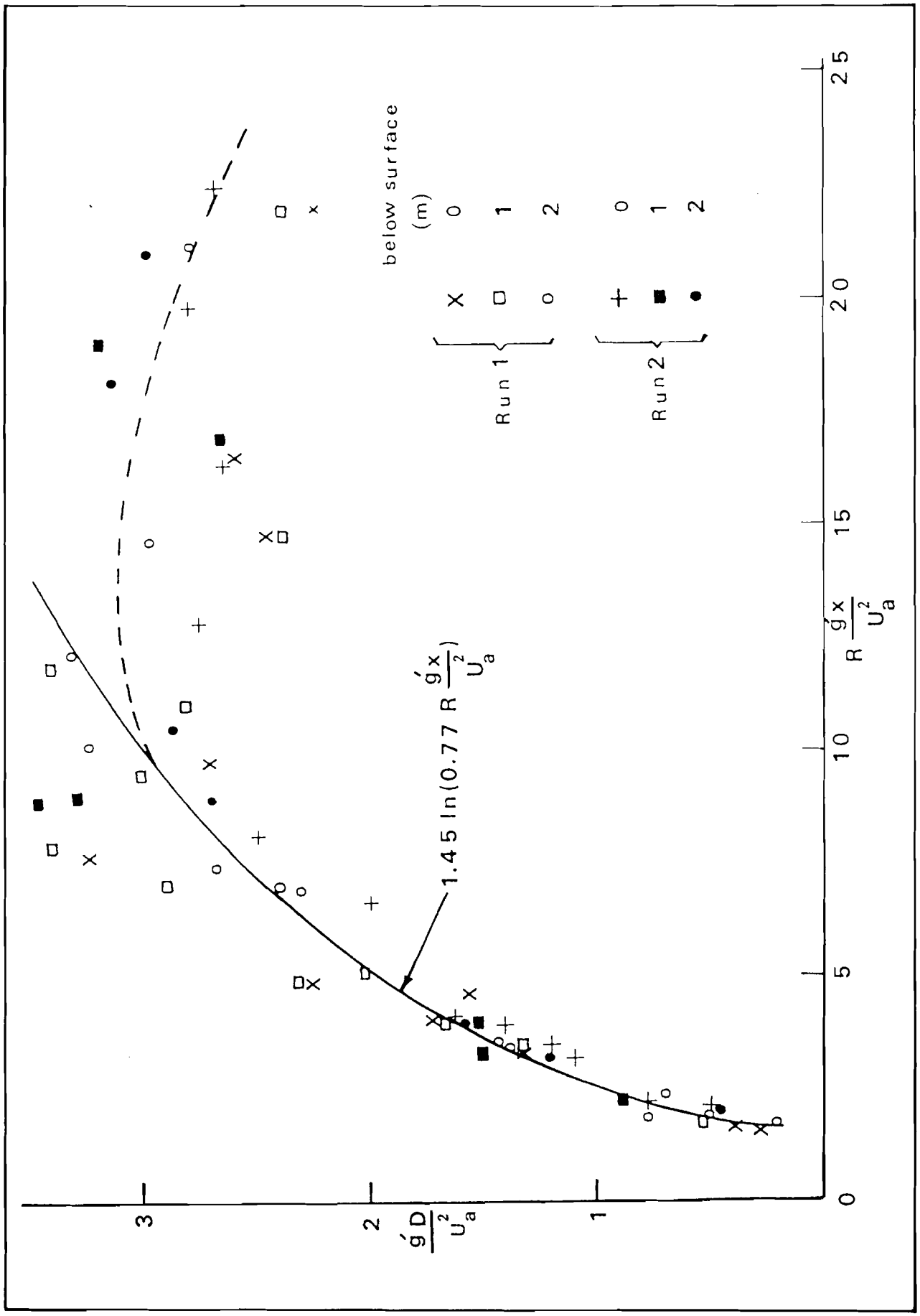

Fig 14 Variation of normalized distance between the right-hand and left-hand side plume axes with downstream distance x (see Fig 4)